PHYSICAL REVIEW D **95,** 015017 (2017)

Exploring collider signatures of the inert Higgs doublet model

Amitava Datta,[1,*] Nabanita Ganguly,[1,†] Najimuddin Khan,[2,‡] and Subhendu Rakshit[2,§]
[1]*Department of Physics, University of Calcutta, 92 Acharya Prafulla Chandra Road, Kolkata 700 009, India*
[2]*Discipline of Physics, Indian Institute of Technology Indore, Khandwa Road, Simrol, Indore 453 552, India*
(Received 10 October 2016; published 23 January 2017)

We revisit the multilepton $(ml) + \not{E}_T + X$ signatures of the inert doublet model (IDM) of dark matter in future LHC experiments for $m = 3, 4$ and simulate, for the first time, the $m = 5$ case. Here X stands for any number of jets. We illustrate these signals with benchmark points consistent with the usual constraints like unitarity, perturbativity, the precision electroweak data, the observed dark matter relic density of the Universe and, most importantly, the stringent LHC constraints from the post–Higgs (h) discovery era like the measured M_h and the upper bound on the invisible width of h decay, which were not included in earlier analyses of multilepton signatures. We find that if the IDM is embedded in a grand desert scenario so that the unitarity constraint holds up to a very high scale, the whole of the highly restricted parameter space allowed by the above constraints can be probed at the LHC via the $3l$ signal for an integrated luminosity $\sim$3000 fb^{-1}. On the other hand, if any new physics shows up at a scale $\sim$10 TeV, only a part of the enlarged allowed parameter space can be probed. The $4l$ and $5l$ signals can help to discriminate among different IDM scenarios as and when sufficient integrated luminosity accumulates.

DOI: 10.1103/PhysRevD.95.015017

I. INTRODUCTION

Discovery of a scalar boson [1,2] at the Large Hadron Collider (LHC) in 2012 with properties very similar to the Higgs boson (h) responsible for electroweak symmetry breaking in the Standard Model (SM) with a minimal scalar sector has validated this model. The mass of the Higgs-like boson has been measured to be about 125 GeV [1–3]. So far, neither the LHC nor other experiments have discovered any signature of new physics beyond the SM. However, the nonzero neutrino masses, the baryon-antibaryon asymmetry in nature, the presence of dark matter (DM) and dark energy in the Universe, and many other observables compel us to look beyond the minimal SM. In this paper our focus will be on a popular model which can potentially explain the measured DM relic density in the Universe [4].

Strong astrophysical evidence suggests that our Universe is pervaded by DM. The relic density of DM is $\Omega h^2 = 0.1198 \pm 0.0026$ as measured by the satellite-based experiments Planck [5] and WMAP [6] that are geared to the measurement of various properties of the cosmic microwave background radiation (CMBR) with an unmatched precision. It will be doubly assuring to confirm the presence of DM by terrestrial experiments. Many such experiments have been carried out for direct detection of DM via its scattering with nucleons [7–9]. However, no signal has been detected. Recent null results by the LUX experiments [7] could eliminate a significant portion of the parameter space in the DM mass versus DM-nucleon cross-section plane. However, these constraints are marred by the uncertainties stemming from the assumption that the Earth is flying through a uniform DM cloud of significant density. The clumpy nature of DM leaves open the possibility that the density of DM in the cosmologically tiny region surrounding the Earth, which has not been directly measured so far, is very small. This makes the option that DM may be produced directly at a high-energy collider like the LHC even more attractive. Weakly interacting massive particles (WIMPs) can indeed be produced by the proton-proton collisions at the LHC which escape the detector, leading to the celebrated missing energy signal. As backgrounds are somewhat better understood in a manmade laboratory, it is not unreasonable to argue that a collider might be the best bet in revealing the true nature of DM particles.

The search for DM at the LHC is a topic of great contemporary interest. A large number of models compatible with the relic density data have been proposed, and their prospective signatures at the LHC have been studied (see, e.g., Refs. [10,11]). The discovery of the Higgs boson [1–3] has completed the spectrum of the minimal version of the SM. Yet it must be admitted that the scalar sector of the SM is the least constrained one [12]. It is, therefore, quite probable that the DM particle has its abode in the extended scalar sector. A simple possibility, which we pursue in this paper, is to extend the scalar sector of the SM by a $SU(2)$ doublet protected by a $\mathbb{Z}_2$ discrete symmetry. This model, known as the inert doublet model (IDM), was first proposed by Deshpande and Ma [13]. In the IDM, heavier neutral and

*adatta_ju@yahoo.co.in
†nabanita.rimpi@gmail.com
‡phd11125102@iiti.ac.in
§rakshit@iiti.ac.in

charged scalars do exist but do not take part in electroweak symmetry breaking. The exact $\mathbb{Z}_2$ symmetry does not allow the heavier neutral scalar to mix with the SM Higgs and as a result, it does not acquire a vacuum expectation value. In this model, the lightest scalar, odd under $\mathbb{Z}_2$, provides the WIMP DM candidate. This particle may be produced in association with a heavier scalar. It may also appear in the decay cascades of the heavier scalars which are produced in pairs. Both processes yield the generic m leptons + n jets + $\not{E}_T$ signatures, where the leptons and jets come mainly from $W^\pm$ and Z bosons which also appear in the above decay cascades. For $m = 0$, the signal is relatively large, but this electroweak jet production is easily swamped by the huge QCD background. As has already been noted in the literature and will be reiterated in this paper, the $\not{E}_T$ in the signal is rather modest, which is not enough to discriminate against the strong QCD backgrounds with cross sections several orders of magnitude larger. It should be borne in mind that in a hadron collider, the latter processes also involve a sizeable $\not{E}_T$ due to the mismeasurement of jet energies, underlying events, etc. The main attention has therefore been focused on multilepton+$\not{E}_T$ signatures. Here one has to contest the electroweak backgrounds with a relatively small cross section. The task, nevertheless, is uphill, as both the signal and the background, which typically has a much larger size, involve leptons coming from $W^\pm$ and Z decays. However, after adjusting the cuts, a modest signal-to-background ratio can be salvaged at the LHC experiments with upgraded luminosity, especially if the signal involves virtual Z's. This will be shown below.

The most well studied signal of the DM-Higgs coupling, both phenomenologically [14–17] and experimentally [18–21], has been the invisible decay of h. This occurs provided the mass of the DM particle is $< M_h/2$. However, since this generic signature may arise in any model where h can decay into a pair of long-lived WIMPs—not necessarily the DM particle—it is hard to figure out the underlying physics from this signal alone. The next simplest case is the dilepton + $\not{E}_T$ topology ($m = 2$). This has already been studied in the context of the IDM [22,23]. It has been noted that the LHC run 1 data in this channel is sensitive only to regions of the parameter space not containing a viable DM candidate [23]. Nevertheless, the authors optimistically expected an observable signal during run 2 [23]. It should, however, be stressed that even if both these signals show up, it will still be difficult to reveal the new physics involved. Additional search channels, therefore, are always welcome.

Signatures with $m = 3, 4$ were studied in the IDM [24,25]. However, the parameter space of the IDM is constrained by a plethora of important constraints, both theoretical and empirical (see Sec. III for references and further details). In Refs. [24,25], the above signals were illustrated with benchmark points (BPs) not compatible with some important LHC constraints in the post–Higgs discovery era like the measurement of the Higgs boson mass, the strong upper bound on the invisible decay width of the Higgs boson [26]. The main emphasis of this paper is to assess the prospect of these signals with a new set of realistic BPs consistent with more recent and stronger constraints. More importantly, we have not restricted our analyses to isolated BPs only. We have identified, as and when possible, the portions of the allowed parameter spaces (APSs) of several representative scenarios sensitive to the proposed signals in future LHC experiments. Then we have illustrated the features of the prospective signals with the help of BPs. Finally, we have studied, for the first time, the $5l + \not{E}_T$ signal.

Unlike some of the earlier analyses, we do not impose any jet veto on the multilepton final states. Generically, therefore, the signatures studied have the topology m leptons + $\not{E}_T$ + X, where X stands for any number of jets. This choice is necessitated by the fact that the leptonic final states arising from the decays of the extra scalars in the IDM are often accompanied by ISR jets, and a good fraction of the signal may be lost if the jet veto is imposed. This strategy is similar to the ones currently adopted by the LHC collaborations for multilepton analyses.

The plan of the paper is as follows: In Sec. II, we briefly review the salient features of the IDM. In the next section, we introduce three representative scenarios in the IDM and study the APS in each case in the light of the available constraints. In Sec. IV, we study the portions of the above APSs which are within the reach of future LHC experiments. Illustrative numerical results in each scenario are provided with the help of several BPs. The main conclusions are summarized in the last section.

II. INERT DOUBLET MODEL

In this model, the Standard Model is extended by adding an extra $SU(2)$ doublet scalar, odd under an additional discrete $\mathbb{Z}_2$ symmetry. Under this symmetry, all Standard Model fields are even. The $\mathbb{Z}_2$ symmetry prohibits the inert doublet from acquiring a vacuum expectation value.

The renormalizable CP-conserving scalar potential at the tree level is given by [13]

$$\begin{aligned} V(\Phi_1,\Phi_2) = {} & \mu_1^2|\Phi_1|^2 + \lambda_1|\Phi_1|^4 + \mu_2^2|\Phi_2|^2 + \lambda_2|\Phi_2|^4 \\ & + \lambda_3|\Phi_1|^2|\Phi_2|^2 + \lambda_4|\Phi_1^\dagger\Phi_2|^2 \\ & + \frac{\lambda_5}{2}[(\Phi_1^\dagger\Phi_2)^2 + \text{H.c.}], \end{aligned} \tag{2.1}$$

where $\mu_{1,2}$ and λ_i ($i = 1, 2, 3, 4, 5$) are real parameters. The SM Higgs doublet Φ_1 and the inert doublet Φ_2 are given by

$$\Phi_1 = \begin{pmatrix} G^+ \\ \frac{1}{\sqrt{2}}(v + h + iG^0) \end{pmatrix}, \qquad \Phi_2 = \begin{pmatrix} H^+ \\ \frac{1}{\sqrt{2}}(H + iA) \end{pmatrix},$$

where $v = 246.221$ GeV is the vacuum expectation value of the Φ_1, $G^\pm$ and G^0 are Goldstone bosons, and h is the SM Higgs.

Φ_2 contains a CP-even neutral scalar H, a CP-odd neutral scalar A, and a pair of charged scalar fields $H^\pm$. The $\mathbb{Z}_2$ symmetry prohibits an *odd* number of these scalar fields coupling with the SM particles. Either of the lightest neutral components H and A is stable and may be considered a DM candidate.

After electroweak symmetry breaking, the scalar potential is given by

$$\begin{aligned} V(h,H,A,H^\pm) &= \frac{1}{4}[2\mu_1^2(h+v)^2+\lambda_1(h+v)^4 \\ &+ 2\mu_2^2(A^2+H^2+2H^+H^-) \\ &+ \lambda_2(A^2+H^2+2H^+H^-)^2] \\ &+ \frac{1}{2}(h+v)^2[\lambda_3 H^+H^- + \lambda_S A^2 + \lambda_L H^2], \end{aligned} \tag{2.2}$$

where

$$\lambda_{L,S} = \frac{1}{2}(\lambda_3+\lambda_4 \pm \lambda_5). \tag{2.3}$$

Masses of these scalars are given by

$$\begin{aligned} M_h^2 &= \mu_1^2 + 3\lambda_1 v^2, \\ M_H^2 &= \mu_2^2 + \lambda_L v^2, \\ M_A^2 &= \mu_2^2 + \lambda_S v^2, \\ M_{H^\pm}^2 &= \mu_2^2 + \frac{1}{2}\lambda_3 v^2. \end{aligned}$$

For $\lambda_4-\lambda_5<0$ and $\lambda_5>0$ ($\lambda_4+\lambda_5<0$ and $\lambda_5<0$), A (H) is the lightest $\mathbb{Z}_2$-odd particle (LOP). In this work, we take A as the LOP and hence, as a viable DM candidate. The choice of H as the LOP will lead to similar results.

For analyses in the next two sections, we define

$$\begin{aligned} \Delta M_H &\equiv M_H - M_A, \\ \Delta M_{H^\pm} &\equiv M_{H^\pm} - M_A \end{aligned}$$

so that the independent parameters for the IDM become $\{M_A, \Delta M_H, \Delta M_{H^\pm}, \lambda_2, \lambda_S\}$. Here we have chosen the Higgs portal coupling λ_S as we treat A as the DM particle. Moreover, λ_2 does not play any role in relic density calculation. Nor does it directly affect the masses of the inert scalars which determine the collider signatures [23]. We have, therefore, chosen $\lambda_2 = 0$.[1]

[1]However, it had been shown in Refs. [27–32] that depending on the parameter space, this choice might lead to a $\mathbb{Z}_2$-violating vacuum at finite temperatures. During the thermal evolution of the Universe, if the Universe happens to rest in such a vacuum for long, it might lead to intriguing cosmological implications [32]. A detailed study of this parameter-space-dependent effect is beyond the scope of this paper.

III. THE CONSTRAINTS ON THE IDM AND THEIR IMPLICATIONS

The five-dimensional parameter space of this model discussed in the last section is constrained by various theoretical considerations like stability of the vacuum, perturbativity, and unitarity of the scattering matrix. Experimental constraints such as the electroweak precision measurements, the direct search limits from LEP, and the Higgs invisible decay width measured at the LHC also impose additional constraints. Last but not the least, the requirement that the IDM alone saturate the measured DM relic density of the Universe is also instrumental in obtaining a finite APS to be tested at the LHC. Recently, detailed bounds on the IDM have been studied by several groups; see e.g. Refs. [33–50].

In this study, we first determine the APS consistent with the above constraints for three representative scenarios:

(A) $M_A = 70.0$ GeV, $\lambda_S = 0.005$ (Fig. 1 of this paper).
(B) $M_A = 70.0$ GeV, $\lambda_S = 0.007$ (Fig. 2 of Ref. [47]).
(C) $M_A = 55.0$ GeV, $\lambda_S = 0.0035$ (Fig. 2 of this paper).

Comparison of scenarios A and B highlights the changes in the APS with λ_S for fixed M_A. On the other hand, scenario C represents a parameter space where invisible Higgs decay is allowed. In all three cases, the free parameters ΔM_H and $\Delta M_{H^\pm}$ delineate the APS restricted by the above constraints. These parameters, along with M_A, govern the prospective LHC signatures in each scenario to be studied in the following. It may be noted that in scenario C, the constraint from the invisible decay width of h requires λ_S to

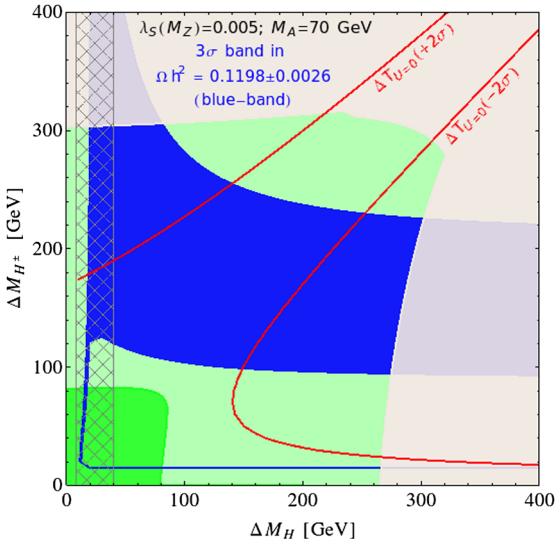

FIG. 1. The allowed parameter space in the ΔM_H–$\Delta M_{H^\pm}$ plane for $M_A = 70$ GeV and $\lambda_S = 0.005$. The constraints from the T parameter allow only the area between the solid red lines. In the green region in the lower-left corner, the unitarity bound is valid up to the Planck scale. In the light green region, the unitarity bound is valid up to 10 TeV. The blue regions are allowed by the DM constraint at the 3σ level [5] and the relaxed unitarity constraint. The cross-hatched region is excluded from LEP II data.

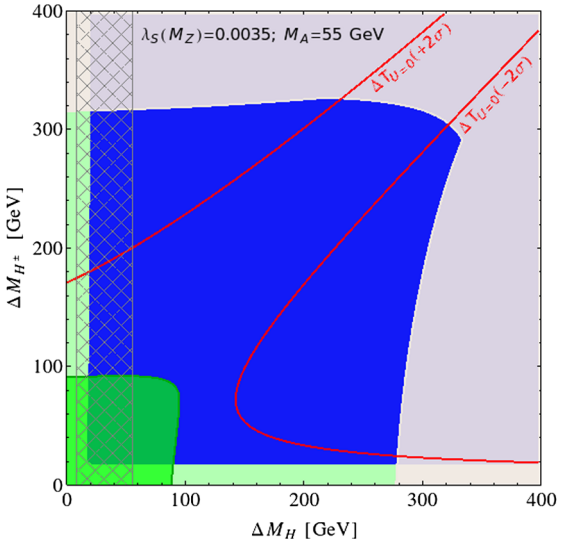

FIG. 2. The allowed parameter space in the ΔM_H–$\Delta M_{H^\pm}$ plane for $M_A = 55$ GeV and $\lambda_S = 0.0035$. The constraints from the T parameter, LEP II, and the stronger unitarity condition are as in Fig. 1. The blue region is allowed by the DM constraint at the 3σ level [5] and the weaker unitarity condition.

be $\sim 10^{-3}$. However, in scenarios A and B, larger λ_S could have been chosen as long as the choice was consistent with the observed DM relic density [5,6]. Of course, much larger λ_S would be in conflict with the bounds from direct DM detection experiments [7]. However, as argued in the Introduction, these bounds are not yet compelling. Nevertheless, we have restricted ourselves to choices consistent with the LUX data. In any case, larger values of λ_S do not change our main results qualitatively.

A. Vacuum stability bounds

The stability of the scalar potential requires that the potential not be unbounded from below; i.e., it should not approach negative infinity along any direction in the field space at large field values. The tree-level scalar potential $V(\Phi_1, \Phi_2)$ is stable and bounded from below if [13]

$$\lambda_{1,2}(\Lambda) \geq 0, \qquad \lambda_3(\Lambda) \geq -2\sqrt{\lambda_1(\Lambda)\lambda_2(\Lambda)},$$
$$\lambda_{L,S}(\Lambda) \geq -\sqrt{\lambda_1(\Lambda)\lambda_2(\Lambda)}, \tag{3.1}$$

where the coupling constants are evaluated at a scale Λ using RG equations. However, for the parameter spaces considered in this paper, the consequences of this bound are covered by other constraints.

B. Perturbativity bounds

For the IDM to behave as a perturbative quantum field theory at any given scale Λ, one must impose conditions on the couplings of radiatively improved scalar potential $V(\Phi_1, \Phi_2)$, as

$$|\lambda_{1,2,3,4,5}| \leq 4\pi. \tag{3.2}$$

These upper bounds on the couplings λ_i at Λ restrict ΔM_H and $\Delta M_{H^\pm}$.

C. Unitarity bounds

The parameters of the scalar potential are severely constrained by the unitarity of the S matrix, which at high energies consists of the quartic couplings λ_i of the scalar potential. At very high field values, one obtains the S matrix by using various scalar-scalar, gauge boson–gauge boson, and scalar–gauge boson scatterings [51]. The unitarity of the S matrix demands that the absolute eigenvalues of the scattering matrix should be less than 8π [52–54] up to a certain scale Λ. In this analysis, we consider two choices of Λ: (i) the Planck scale, and (ii) 10 TeV. The former choice, representing the case where the IDM is the low-energy sector of a grand desert model, imposes very strong constraints on the allowed region in the ΔM_H–$\Delta M_{H^\pm}$ plane, as can be seen from the bounded regions in the lower-left corners of Fig. 1 (scenario A) and Fig. 2 (scenario C) of this paper, as well as Fig. 2 (scenario B) and Fig. 5 of Ref. [47].[2] It also follows by comparing these figures that for small λ_S, this constraint is fairly insensitive to the choice of λ_S. For the latter, the choice of scale signifies the onset of some beyond-IDM physics at a scale ~ 10 TeV. Here the relaxed unitarity constraints are much weaker, leading to a larger APS in each case, as is illustrated by the light green region of Fig. 1 and the blue region in Fig. 2.[3] We have checked that the entire parameter space shown in Fig. 2 of Ref. [47] is allowed by the relaxed unitarity constraint.

D. Bounds from electroweak precision experiments

Electroweak precision data has imposed bounds on the IDM via the Peskin-Takeuchi [55] parameters S, T, U, and the contributions of the additional scalars of the IDM to these parameters can be found in Refs. [52,56]. We use the NNLO global electroweak fit results obtained by the Gfitter group [57],

$$\Delta S = 0.06 \pm 0.09, \qquad \Delta T = 0.1 \pm 0.07, \tag{3.3}$$

with a correlation coefficient of $+0.91$, for ΔU to be zero. We use Eq. (3.3), as the contributions of the scalars in the IDM to ΔU are indeed negligible. In Fig. 1, Fig. 2, and Fig. 2 of Ref. [47], the parameter space allowed by the ΔT constraint at the 2σ level is the region between the two red solid curves (the same color convention has been used in all figures). This constraint is roughly independent of λ_S.

[2]We caution the reader that the color conventions are not the same in different figures.

[3]The narrow gaps beyond the left and the lower edges of the blue region in Fig. 2 are due to the DM constraint, as we shall see below.

The entire parameter space in Fig. 1 is allowed by the ΔS constraint at the 2σ level. It is well known that the ΔT constraint primarily restricts the $SU(2)$-breaking parameter ΔM_H and $\Delta M_{H^\pm}$. However, it should be borne in mind that large values of these mass differences, though allowed by the electroweak precision data, are forbidden by the perturbativity and unitarity constraints. This results in an APS bounded from above, as is illustrated in the above figures.

E. Bounds from LHC diphoton signal strength

In the IDM, the $H^\pm$ gives additional contributions to the diphoton decay of the Higgs at one loop. The analytical expressions can be found in Refs. [58–60]. The measured values are $\mu_{\gamma\gamma} = 1.17 \pm 0.27$ from ATLAS [61] and $\mu_{\gamma\gamma} = 1.14^{+0.26}_{-0.23}$ from CMS [62]. The benchmark points used in this paper are allowed at 1.5σ by both the experiments.

F. Invisible Higgs decay bounds from the LHC

If the inert particle mass is less than $\frac{M_h}{2}$, then the Higgs can decay to a pair of inert particles. LHC's invisible Higgs decay [18–20] width puts stringent constraints on the parameter spaces for inert particle mass less than $\frac{M_h}{2}$. For more details, see Refs. [36,47,63]. In scenario C, the BR of invisible h decay is approximately 0.05. In Fig. 3, we illustrate the parameter space where relic density is in the right ballpark as a function of DM masses for three choices of λ_s.

G. Direct search limits from LEP

The decays $Z \to AH$, $Z \to H^+H^-$, $W^\pm \to AH^\pm$, and $W^\pm \to HH^\pm$ are restricted from Z and $W^\pm$ decay widths at LEP. It implies $M_A + M_H \geq M_Z$, $2M_{H^\pm} \geq M_Z$, and $M_{H^\pm} + M_{H,A} \geq M_W$. More stringent constraints on the IDM can be extracted from chargino [64] and neutralino [65] searches at LEP II. The charged Higgs mass $M_{H^\pm} \geq 70$ GeV. The bound on M_A is rather involved: If $M_A < 80$ GeV, then ΔM_H should be either ≤ 8 GeV or $\gtrsim 110$ GeV (see Fig. 7 of Ref. [65]).

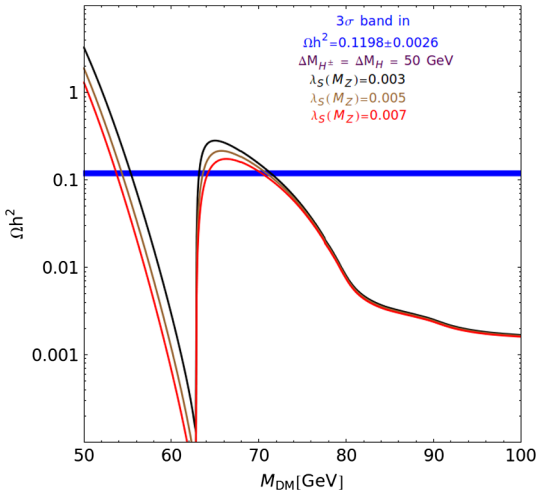

FIG. 3. The DM relic density Ωh^2 as a function of the DM mass $M_{\rm DM}(\equiv M_A)$ for different values of the coupling: $\lambda_S(M_Z) = 0.003$ (black), 0.005 (brown), and 0.007 (red), with $\Delta M_{H^\pm} = \Delta M_H = 50$ GeV. The thin blue band corresponds to the observed DM relic density of the Universe at the 3σ level.

H. Constraints from dark matter relic density

In the relic density calculation, the parameters $\{M_A, \Delta M_H, \Delta M_{H^\pm}, \lambda_S\}$ play pivotal roles. In this model, DM masses below 50 GeV are excluded by the measured DM relic density of the Universe and the invisible decay width [66] of the Higgs from the LHC global fit [26]. For $50 < M_A < 75$ GeV (see Fig. 3) and $M_A \gtrsim 500$ GeV, we get a DM relic density in the right ballpark. However, we do not pursue the heavy-M_A option any further, as it does not lead to interesting LHC signatures. For further details, we refer the reader to Refs. [47,63]. In Fig. 1 (scenario A), the upper and the narrow lower blue bands correspond to relic densities allowed by Planck [5] and WMAP [6] data within 3σ for $M_A = 70$ GeV and $\lambda_S = 0.005$. The dominant contribution comes from the process $AA \to W^\pm W^{\mp *}$,[4] although the process $AA \to ZZ^*$ also contributes modestly. When $M_H/M_{H^\pm}$ is close to the DM mass (the narrow blue bands in Fig. 1), the contributions coming from coannihilation [67] between A, H/A, $H^\pm$ are also significant [68]. Due to the stronger unitarity constraint up to the Planck scale (see the darker green region of Fig. 1), only the thin lower blue band is allowed. If instead the weaker unitarity constraint is imposed, then a sizeable part of the upper blue band is also allowed. Comparing with Fig. 2 of Ref. [47], it follows that for a larger λ_S ($= 0.007$), the upper blue band shifts downwards along the $\Delta M_{H^\pm}$ axis. In this case, the enhanced contributions coming from h-mediated s-channel processes allow the lower values of $\Delta M_{H^\pm}$. However, ΔM_H remains almost unchanged. On the other hand, for still smaller λ_S (e.g., 0.001), the DM constraints allow only narrow strips in the parameter space (see Fig. 5 of Ref. [47]). It is worth noting that the apparently large APS, which opens up due to the relaxation of unitarity constraints, is severely reduced by the very tight relic density constraints resulting in an APS bounded from above. In scenario C (Fig. 2), the main contribution to the relic density comes from the process $AA \to b\bar{b}$ via h exchange. The parameter space allowed by the DM constraint in this case is much larger compared to that of the other scenarios. The entire $\Delta M_{H^\pm} - \Delta M_H$ plane for $\Delta M_{H^\pm}$, $\Delta M_H \gtrsim 12$ GeV is allowed by WMAP and Planck data. Of course, the unitarity bounds and the T-parameter constraints restore a finite APS.

We conclude by noting that the allowed parameter space of the IDM is severely restricted by the perturbativity,

[4]The virtual $W^{\pm *}$ decays to quarks and leptons.

unitarity, electroweak precision data, and DM relic density constraints, resulting in a bounded APS in all the scenarios we have studied. In the next section, we turn our attention to the LHC signatures viable in these APSs, and to illustrating the signatures with benchmark points consistent with all constraints.

IV. THE MULTILEPTON SIGNATURES AT THE LHC

Due to the $\mathbb{Z}_2$ symmetry, the inert scalars are produced in pairs. The dominant production processes at the LHC are $H^\pm H$, $H^\pm A$, and H^+H^-. The heavier scalar $H^\pm$ (H) eventually decays into the SM gauge boson W (Z) and the stable inert scalar A that escapes the detector, giving rise to $\not{E}_T$. Depending on the decay modes of W, Z, various final states can be observed at future LHC experiments (e.g. jets + $\not{E}_T$, leptons + $\not{E}_T$, jets + leptons + $\not{E}_T$). For reasons discussed in the Introduction, we focus on the m leptons + $\not{E}_T + X$ topologies with $m = 3$, 4, and 5, where X stands for any number of jets. Thus, if some of the gauge bosons in the final state provide the required number of leptons, the others decay hadronically.

In our analysis, we have used `FeynRules` [69] to generate IDM model files and `micrOMEGAs` [70] to calculate the relic density of A. Signal events are generated using `CALCHEP 3.6.23` [71] and hadronization, and showering is done by `PYTHIA 6.4` [72], using a `CALCHEP-PYTHIA` interface. Each background event is generated with one extra jet at parton level using ALPGEN [73] with an MLM matching [74] scheme to avoid double counting of jets and then passed to `PYTHIA` for hadronization and showering. Jets are reconstructed using Fastjet [75] with an anti-K_T [76] algorithm using the size parameter $R = 0.5$, a jet P_T threshold of 20 GeV, and $|\eta| < 2.5$. Each lepton is selected with $P_T > 10$ GeV, $|\eta| < 2.5$ and is required to pass the isolation cuts as defined by the ATLAS and CMS collaborations [77,78]. We have used CTEQ6L [79] for parton distribution functions for all our simulations.

A. The $3l + \not{E}_T$ signal

First, we concentrate on the $3l + \not{E}_T + X$ final state. The dominant contribution comes from the processes

(1) $pp \to H^\pm H$, followed by $H^\pm \to W^\pm A/W^\pm H$, $H \to ZA$. However, depending on $\Delta M_{H^\pm H} = |M_{H^\pm} - M_H|$, the following processes may also contribute:
(2) $pp \to H^\pm A$, followed by $H^\pm \to W^\pm H$, $H \to ZA$.
(3) $pp \to H^\pm H^\mp$ followed by $H^\pm \to W^\pm H/W^\pm A$.

$W^\pm$ and Z decay into leptons ($W^\pm \to l^\pm \nu, Z \to l^+l^-$), where l stands for e or μ. Here $H^\pm$ decays to $W^\pm A$ with a branching ratio (BR) of almost 100% for $M_{H^\pm} > (M_W + M_A)$. For lower $M_{H^\pm}$, the decay can occur via a virtual $W^\pm$ boson. $H^\pm$ can also decay into $HW^\pm$ with sufficiently large BRs if the decay is kinematically allowed. In most cases, H will decay into ZA with 100% BR, where Z can be either off shell or on shell depending on ΔM_H. However, if $M_H > M_{H^\pm}$, $H \to W^\mp H^\pm$ may be a competing mode.

The dominant SM backgrounds giving trilepton final states are

(1) $W^\pm Z$ production, where both $W^\pm$ and Z decay into leptons.
(2) ZZ production, followed by leptonic decays of both Z bosons.
(3) $t\bar{t}Z$, followed by $Z \to l^+l^-$, $t(\bar{t}) \to b(\bar{b})W^+(W^-)$, and one of the two W's decays into leptons.
(4) VVV (where $V = W^\pm, Z$) production, where leptonic decays of $W^\pm$, Z may lead to final states with $3l + \not{E}_T$.

In this paper, we focus on the experiments at 13 TeV. In order to suppress the large SM background, we have employed the following cuts:

(1) Exactly three isolated leptons are required.
(2) $\not{E}_T > 100$ GeV.
(3) If the invariant mass of any SFOS (same-flavor opposite-sign) pair of leptons is found to be in the range 81.2–101.2 GeV, the event is rejected.

The dominant WZ background inevitably contains an on-shell Z boson—i.e., the invariant mass distribution of a SFOS lepton pair peaks around M_Z. This immediately suggests that the last cut can suppress the background significantly if the signal events do not contain an on-shell Z boson. The number of background events after all cuts is 4039.8 for an integrated luminosity of 3000 fb^{-1}.

We have introduced in Sec. III three representative scenarios: A, B, and C. Benchmark points (BP1–BP12) satisfying all constraints discussed in Sec. III are chosen from these scenarios and displayed in Table I. The relevant production cross sections and BRs are listed in Table II. From this information it readily follows that the event rates for different multilepton signals before applying the kinematical selections is already modest. Moreover, the spectra of the additional scalars are somewhat compressed due to the constraints discussed in the last section. As a result, the $\not{E}_T$ spectra of various signals tend to be rather soft. This is why one has to wait for a sufficiently large integrated luminosity for observing the signals, as we shall see in the current section.

We begin with scenario B (Fig. 2 of Ref. [47]) with $\lambda_S = 0.007$ and $M_A = 70$ GeV (see BP1–BP4). If we require unitarity up to the Planck scale (i.e. a grand-desert-type scenario), a tiny part of the total parameter space (the white region in the lower-left corner of Fig. 2 of Ref. [47]) survives. The intersection of this region with the parameter space allowed by the DM (the upper and lower blue bands), the T parameter, and other constraints constitutes the APS. In the entire APS, both W and Z bosons in the signal are off shell, since $\Delta M_{H^\pm}$ and ΔM_H are relatively small. This, as discussed above, enables one to probe the whole APS via the

TABLE I. A list of the BPs used in our analysis.

Benchmark		Masses in GeV		
points	λ_S	M_A	$M_{H^\pm}$	M_H
BP1			85	140
BP2	0.007	70	120	150
BP3			150	140
BP4			170	120
BP5			200	150
BP6	0.005	70	240	130
BP7			260	120
BP8			280	160
BP9			75	135
BP10	0.0035	55	175	125
BP11			235	115
BP12			265	115

trilepton signal at the LHC with an integrated luminosity of $\approx$3000 fb^{-1}. The significance of the signal for BP1 belonging to the lower narrow blue band (see Table III) is encouraging. Similar promising results for BP2 and BP3 in the upper blue band are also in the same table.

As already noted in Sec. III, if the scale of the validity of the unitarity constraint is relaxed to 10 TeV, assuming this to be the onset of some new physics, the entire parameter space shown in Fig. 2 of [47] becomes consistent with this relaxed constraint. Consequently, the entire broader blue band, subject to the T parameter and other constraints, belongs to the APS. However, only points with $\Delta M_H \leq M_Z$ can be probed at the LHC as has already been noted. On the other hand, almost all $M_{H^\pm}$ allowed by the vertical width of the APS can be probed by the future LHC experiments with integrated luminosity 3000 fb^{-1}. In Table III, BP4 near the upper edge of the APS illustrates the significance of the signal.

In scenario A, represented by BP5–BP8, the upper blue band allowed by the DM constraint is shifted to higher $\Delta M_{H^\pm}$ compared to that in scenario B (see Fig. 1). As a result, the stronger unitarity, the DM, and the T-parameter constraints allow a small APS consisting of a part of the horizontal blue band corresponding to $\Delta M_{H^\pm} \approx 15$ GeV. Similar conclusions hold for still smaller λ_S, as can be seen from Fig. 5 of Ref. [47] with $\lambda_S = 0.001$. In all such cases, the entire APS can be probed by the LHC experiments at 13 TeV with an integrated luminosity of about 3000 fb^{-1}. If, instead, the weaker unitarity constraint is invoked, the APS includes a part of the broader blue region in Fig. 1 consistent with all constraints. The portion corresponding to $\Delta M_H < M_Z$ can be probed, as is illustrated by BP5–BP8 in Table III. Note that for BP6–BP8, $\Delta M_{H^\pm H}$ is larger than M_W, so that the decay $H^\pm \to HW$ is kinematically allowed and occurs with fairly large BR (see Table II). As a result, the pair-production processes $H^\pm H$, $H^\pm A$, and H^+H^- can contribute to the $3l + \not{E}_T + X$ signal. These processes are also potential sources of the $4l$ and $5l$ signatures, which will be discussed below. It can be readily seen from Fig. 1 that for $\Delta M_{H^\pm} \gtrsim 210$ GeV, the T-parameter constraint implies that H necessarily decays into on-shell Z bosons. Thus, in this scenario, $M_{H^\pm} \leq 280$ GeV can be probed by the future LHC experiments for the above integrated luminosity. This is illustrated by BP8 in Table III. As discussed above,

TABLE II. Leading-order cross sections (in fb) for $H^\pm H$, $H^\pm A$, and H^+H^- production processes at $\sqrt{s} = 13$ TeV and their leptonic BRs for BPs defined in Table I. For each BP, only the processes that can lead to ≥ 3 leptons in the final state are shown. "…" indicates that the process cannot give multileptons, and "$*$" indicates that the corresponding decay mode is absent.

Cross sections	Benchmark points					
and BRs	BP1	BP2	BP3	BP4	BP5	BP6
$H^\pm H$	235.8	124.7	96.73	94.97	47.72	37.09
$H^\pm A$	…	…	…	…	…	61.78
H^+H^-	…	…	…	…	…	10.07
$H^\pm \to l^\pm \nu A$	0.226	0.226	0.225	0.224	0.226	0.188
$H^\pm \to l^\pm \nu H$	$*$	$*$	$*$	$*$	$*$	0.042
$H \to l^+l^-A$	0.037	0.067	0.069	0.069	0.069	0.069
$H \to l^\pm \nu H^\mp$	0.101	$*$	$*$	$*$	$*$	$*$
Cross sections	Benchmark points					
and BRs	BP7	BP8	BP9	BP10	BP11	BP12
$H^\pm H$	32.49	19.42	298.7	84.0	44.76	32.05
$H^\pm A$	47.95	37.70	…	…	74.31	49.91
H^+H^-	7.72	6.07	…	…	10.94	7.35
$H^\pm \to l^\pm \nu A$	0.15	0.183	0.225	0.224	0.168	0.148
$H^\pm \to l^\pm \nu H$	0.070	0.036	$*$	$*$	0.052	0.071
$H \to l^+l^-A$	0.069	0.069	0.042	0.069	0.069	0.069
$H \to l^\pm \nu H^\mp$	$*$	$*$	0.044	$*$	$*$	$*$

TABLE III. The number of $3l$ events (denoted by S) surviving the cuts defined in the text, and also the statistical significance (defined as $S/\sqrt{B}$) at $\sqrt{s} = 13$ TeV for an integrated luminosity of 3000 fb^{-1}, are given for all BPs defined in Table I. The number of the total SM background (denoted by B) is 4039.8. The numbers in parentheses represent the statistical significance for 300 fb^{-1} of integrated luminosity.

Benchmark points	Signal events after cuts (S)	$S/\sqrt{B}$	Benchmark points	Signal events after cuts (S)	$S/\sqrt{B}$
BP1	405.0	6.37 (2.01)	BP7	502.3	7.90 (2.50)
BP2	535.8	8.42 (2.66)	BP8	373.7	5.87 (1.85)
BP3	442.2	6.95 (2.19)	BP9	641.5	10.1 (3.19)
BP4	298.8	4.70 (1.48)	BP10	491.6	7.73 (2.44)
BP5	372.0	5.85 (1.85)	BP11	676.6	10.64 (3.36)
BP6	472.8	7.43 (2.35)	BP12	617.8	9.72 (3.07)

lowering λ_S shifts the broader blue band upwards. As a result, the part of the APS accessible to LHC will further shrink for smaller λ_S.

Next, we discuss scenario C with $M_A = 55$ GeV and $\lambda_S = 0.0035$. In the APS compatible with the strong unitarity condition, the LEP, and the DM constraints (see Fig. 2), we have $\Delta M_H < M_Z$. Thus, the entire allowed region can be probed with integrated luminosity 3000 fb^{-1}. If instead the relaxed unitarity is imposed, then the APS is larger (see Fig. 2). If $\Delta M_H < M_Z$ is required for a healthy signal, $\Delta M_{H^\pm}$ must be in the range 12–210 GeV. BP9–BP12 in Table I illustrate this. For BP9 and BP10, $H^\pm$ is much heavier than H, leading to the decay $H^\pm \to WH$ with appreciable BR. On the other hand, for BP11, H is heavier; its decay into $H^\pm W$ with a BR large enough for a multilepton signal is allowed. BP12 represents the reach in $M_{H^\pm}$. This scenario can potentially lead to the invisible Higgs decay signal. Additional confirmation may indeed come from the multilepton signatures.

In Table III, we summarize our results for the $3l + \not{E}_T$ final state assuming an integrated luminosity of 3000 fb^{-1}, where the total SM background (B) is found to be 4039.8. For almost all the BPs, the significance of the signal exceeds 5σ, which indicates a good chance of discovery in future LHC experiments. The numbers in brackets indicate the signal significance for 300 fb^{-1} of integrated luminosity. Note that some of them highlight early hints of new physics at the LHC.

B. $4l + \not{E}_T$ signal

In this section, we discuss the $4l + \not{E}_T + X$ signatures. The dominant contributions to the signal come from the following processes:

(1) $pp \to H^\pm H$, followed by $H^\pm \to W^\pm H$ and $H \to l^+ l^- A$.
(2) $pp \to H^+ H^-$, where either both H^+ and H^- decay into $W^+ H$, or one decays into $W^- H$ and other into $W^\pm A$.

The main SM backgrounds are the following:

(1) ZZ production, followed by the leptonic decays of both Z bosons, $Z \to l^+ l^-$.
(2) $W^\pm W^\mp Z$ production, where both $W^\pm$ and Z decay leptonically, $W^\pm \to l^\pm \nu$ and $Z \to l^+ l^-$.
(3) $W^\pm ZZ$ production, where two Z bosons decay into lepton pairs.
(4) ZZZ production, followed by leptonic decays of any two Z bosons.
(5) Finally, $t\bar{t}Z$ production, followed by $Z \to l^+ l^-$ and $t(\bar{t}) \to b(\bar{b})W^+(W^-)$, $W^\pm \to l^\pm \nu$.

We apply the following set of cuts in our analysis to suppress the background as well as to select signal events:

(1) Exactly four isolated leptons are required.
(2) A cut of 80 GeV on $\not{E}_T$. Note that this cut is strong enough to suppress the potentially strong background coming from ZZ, which has a comparatively soft $\not{E}_T$ distribution.
(3) Finally, an event with at least one SFOS lepton pair with invariant mass in the range 81.2–101.2 GeV is rejected.

After applying the above cuts, the number of total background events (B) reduces to 36.9 for 3000 fb^{-1} of integrated luminosity.

Table IV shows the simulation results corresponding to the BPs introduced in Table I. In many cases, observable signals with an integrated luminosity somewhat larger than the typical choice of 3000 fb^{-1} may be expected.

TABLE IV. Number of $4l$ events (S) along with the statistical significances at $\sqrt{s} = 13$ TeV for an integrated luminosity of 3000 fb^{-1}. BPs are taken from Table I. The number of the SM background (B) is 36.9.

Benchmark points	Signal events after cuts (S)	$S/\sqrt{B}$	Benchmark points	Signal events after cuts (S)	$S/\sqrt{B}$
BP6	21.49	3.53	BP11	31.83	5.30
BP7	21.16	3.45	BP12	27.65	4.55
BP8	9.79	1.59			

TABLE V. Number of $5l$ events (S) at $\sqrt{s} = 13$ TeV for an integrated luminosity of 3000 fb^{-1} for the BPs defined in Table I. The SM background is negligible.

Benchmark points	Signal events after cuts (S)	Benchmark points	Signal events after cuts (S)
BP6	3.33	BP11	5.37
BP7	3.89	BP12	1.92
BP8	1.75		

C. $5l + \not{E}_T$ signal

In this section, we examine the prospects for the $5l + \not{E}_T + X$ signal at future LHC experiments. The main process contributing to the signal is

$$pp \to H^{\pm}H, \text{ followed by } H^{\pm} \to W^{\pm}H, W^{\pm} \to l^{\pm}\nu \text{ and } H \to l^{+}l^{-}A.$$

Note that H^+ pair production (where both H^+ and H^- decay into WH), in principle, can also give $5l$ final states. But we have found this contribution to be negligible. We list below the SM backgrounds:

(1) ZZZ production, followed by leptonic decays of all Z bosons, where one lepton is not detected or fails to pass the cuts.
(2) $W^{\pm}ZZ$ production, with both $W^{\pm}$ and Z decaying into leptons.
(3) $t\bar{t}Z$ production, where the corresponding decay occurs via $Z \to l^{+}l^{-}$, $t(\bar{t}) \to b(\bar{b})W^{+}(W^{-})$, $W^{\pm} \to l^{\pm}\nu$, and one lepton comes from b decay ($b \to cl\nu$).

Demanding five isolated leptons in the final state drastically reduces the background. A cut of 80 GeV on $\not{E}_T$ is good enough to efficiently reduce the background to a negligible level. As a rough guideline, we require for discovery at least five background-free events. We present the results in Table V.

As we see from Table V, when BP11 has a potential discovery chance at $\sqrt{s} = 13$ TeV, the rest of the BPs may provide hints for the IDM at the LHC until higher luminosities well beyond 3000 fb^{-1} accumulate. It also follows from Tables III–V that the relative rates of different signals can discriminate among different IDM scenarios.

V. CONCLUSION

The aim of this paper is to revisit the prospect of observing the $ml + \not{E}_T + X$ signatures predicted by the IDM, a popular DM model, in future LHC experiments for $m = 3, 4$. It may be recalled that the earlier studies [24,25] were based on BPs disfavored by the strong LHC constraints in the post–Higgs discovery era. In this context, the accurate measurement of the Higgs boson mass and the stringent upper bound on the invisible width of the Higgs boson deserve special mentioning. We also simulate for the first time the $5l + \not{E}_T$ signal and study its observability.

To facilitate our analyses, we introduce at the beginning of Sec. III three representative scenarios A, B, and C, and delineate the APS in each case subject to the constraints discussed in the same section (see Fig. 1, Fig. 2, and Fig. 2 of Ref. [47]). Following the search strategies in Sec. IV, we then assess the prospect of discovery of each signal. As discussed in that section, the signals are viable only if the leptons come from the virtual Z bosons (i.e., $\Delta M_H = M_H - M_A < M_Z$). If the IDM is embedded in a grand-desert-type scenario—i.e., the unitarity constraint is required to be valid up to, e.g., the Planck scale—then in each scenario, the APS is tiny with $\Delta M_H < M_Z$. Thus, the entire allowed parameter space in all scenarios can be probed via the $3l$ signal for integrated luminosity $\sim$3000 fb^{-1}. Although one has to wait for the LHC experiments after the third long shutdown to achieve this, these results shows that the grand-desert-type IDM models are definitely falsifiable.

If the unitarity constraint is relaxed to a lower scale, the APS, as expected, is larger in each case. For $\Lambda = 10$ TeV, we have shown that the entire APS (i.e., the allowed range of $\Delta M_{H^{\pm}}$, with $\Delta M_H < M_Z$) is accessible to the LHC experiments in all three scenarios with $\sim$3000fb^{-1} of integrated luminosity. We also point out that the accessible region shrinks for smaller λ_S due to the strong T-parameter constraint.

The above observations are substantiated by numerical results (see Tables III–V) for the BPs in Table I. The relative rates of different ml signals can discriminate among different scenarios.

ACKNOWLEDGMENTS

The research of A. D. was supported by the Indian National Science Academy, New Delhi. N. G. thanks the Board of Research in Nuclear Sciences, Department of Atomic Energy, India, for a research fellowship. The work of N. K. is supported by a fellowship from the University Grants Commission, India. S. R. is funded by the Department of Science and Technology, India, via Grant No. EMR/2014/001177. S. R. acknowledges Siddhartha Karmakar for discussion.

[1] G. Aad *et al.* (ATLAS Collaboration), Observation of a new particle in the search for the Standard Model Higgs boson with the ATLAS detector at the LHC, Phys. Lett. B **716**, 1 (2012).

[2] S. Chatrchyan *et al.* (CMS Collaboration), Observation of a new boson at a mass of 125 GeV with the CMS experiment at the LHC, Phys. Lett. B **716**, 30 (2012).

[3] P. P. Giardino, K. Kannike, I. Masina, M. Raidal, and A. Strumia, The universal Higgs fit, J. High Energy Phys. 05 (2014) 046.

[4] H. Baer and X. Tata, in *Physics at the Large Hadron Collider, Indian National Science Academy, A Platinum Jubilee Special Issue*, edited by A. Datta, B. Mukhopadhyaya, and A. Raychaudhuri (Springer, New York, 2009).

[5] P. A. R. Ade *et al.* (Planck Collaboration), Planck 2013 results: XVI. Cosmological parameters, Astron. Astrophys. **571**, A16 (2014).

[6] C. L. Bennett *et al.* (WMAP Collaboration), Nine-year Wilkinson microwave anisotropy probe (WMAP) observations: Final maps and results, Astrophys. J. Suppl. Ser. **208**, 20 (2013).

[7] D. S. Akerib *et al.* (LUX Collaboration), First Results from the LUX Dark Matter Experiment at the Sanford Underground Research Facility, Phys. Rev. Lett. **112**, 091303 (2014).

[8] E. Aprile *et al.* (XENON100 Collaboration), Dark Matter Results from 100 Live Days of XENON100 Data, Phys. Rev. Lett. **107**, 131302 (2011).

[9] E. Aprile *et al.* (XENON100 Collaboration), Dark Matter Results from 225 Live Days of XENON100 Data, Phys. Rev. Lett. **109**, 181301 (2012).

[10] D. Abercrombie *et al.*, Dark matter benchmark models for early LHC run 2 searches: Report of the ATLAS/CMS dark matter forum, arXiv:1507.00966.

[11] J. Abdallah *et al.*, Simplified models for dark matter searches at the LHC, Phys. Dark Univ. **9–10**, 8 (2015).

[12] CMS Collaboration, Report No. CMS-PAS-HIG-15-002; ATLAS Collaboration, Phys. Lett. B **753**, 69 (2016).

[13] N. G. Deshpande and E. Ma, Pattern of symmetry breaking with two Higgs doublets, Phys. Rev. D **18**, 2574 (1978).

[14] A. Drozd, B. Grzadkowski, and J. Wudka, Multi-scalar-singlet extension of the Standard Model: The case for dark matter and an invisible Higgs boson, J. High Energy Phys. 04 (2012) 006; Erratum, J. High Energy Phys. 11 (2014) 130(E).

[15] M. Battaglia, D. Dominici, J. F. Gunion, and J. D. Wells, The invisible Higgs decay width in the add model at the LHC, arXiv:hep-ph/0402062.

[16] S. Gopalakrishna, S. J. Lee, and J. D. Wells, Dark matter and Higgs boson collider implications of fermions in an Abelian-gauged hidden sector, Phys. Lett. B **680**, 88 (2009).

[17] D. Ghosh, R. Godbole, M. Guchait, K. Mohan, and D. Sengupta, Looking for an invisible Higgs signal at the LHC, Phys. Lett. B **725**, 344 (2013).

[18] G. Aad *et al.* (ATLAS Collaboration), Search for invisible decays of a Higgs boson using vector-boson fusion in pp collisions at $\sqrt{s} = 8$ TeV with the ATLAS detector, J. High Energy Phys. 01 (2016) 172.

[19] CMS Collaboration, Report No. CMS-PAS-HIG-16-009.

[20] S. Chatrchyan *et al.* (CMS Collaboration), Search for invisible decays of Higgs bosons in the vector boson fusion and associated ZH production modes, Eur. Phys. J. C **74**, 2980 (2014).

[21] D. Trocino (CMS Collaboration), Searches for invisible decay modes of the Higgs boson with the CMS detector, Nucl. Part. Phys. Proc. **273–275**, 758 (2016).

[22] E. Dolle, X. Miao, S. Su, and B. Thomas, Dilepton signals in the inert doublet model, Phys. Rev. D **81**, 035003 (2010).

[23] G. Belanger, B. Dumont, A. Goudelis, B. Herrmann, S. Kraml, and D. Sengupta, Dilepton constraints in the inert doublet model from run 1 of the LHC, Phys. Rev. D **91**, 115011 (2015).

[24] M. Gustafsson, S. Rydbeck, L. Lopez-Honorez, and E. Lundstrom, Status of the inert doublet model and the role of multileptons at the LHC, Phys. Rev. D **86**, 075019 (2012).

[25] X. Miao, S. Su, and B. Thomas, Trilepton signals in the inert doublet model, Phys. Rev. D **82**, 035009 (2010).

[26] G. Belanger, B. Dumont, U. Ellwanger, J. F. Gunion, and S. Kraml, Global fit to Higgs signal strengths and couplings and implications for extended Higgs sectors, Phys. Rev. D **88**, 075008 (2013).

[27] I. F. Ginzburg, K. A. Kanishev, M. Krawczyk, and D. Sokolowska, Evolution of Universe to the present inert phase, Phys. Rev. D **82**, 123533 (2010).

[28] D. Sokolowska, Temperature evolution of physical parameters in the inert doublet model, arXiv:1104.3326.

[29] D. Sokolowska, Dark matter data and constraints on quartic couplings in IDM, arXiv:1107.1991.

[30] D. Sokolowska, Dark matter data and quartic self-couplings in inert doublet model, Acta Phys. Pol. B **42**, 2237 (2011).

[31] M. Krawczyk, D. Sokolowska, and B. Swiezewska, Inert doublet model with a 125 GeV Higgs, arXiv:1304.7757.

[32] I. F. Ginzburg, I. P. Ivanov, and K. A. Kanishev, The evolution of vacuum states and phase transitions in 2HDM during cooling of Universe, Phys. Rev. D **81**, 085031 (2010).

[33] L. Lopez Honorez, E. Nezri, J. F. Oliver, and M. H. G. Tytgat, The inert doublet model: An archetype for dark matter, J. Cosmol. Astropart. Phys. 02 (2007) 028.

[34] L. Lopez Honorez and C. E. Yaguna, A new viable region of the inert doublet model, J. Cosmol. Astropart. Phys. 01 (2011) 002.

[35] T. Hambye, F.-S. Ling, L. Lopez Honorez, and J. Rocher, Scalar multiplet dark matter, J. High Energy Phys. 07 (2009) 090; Erratum, J. High Energy Phys. 05 (2010) 66.

[36] A. Arhrib, Y. L. S. Tsai, Q. Yuan, and T. C. Yuan, An updated analysis of inert Higgs doublet model in light of the recent results from LUX, PLANCK, AMS-02 and LHC, J. Cosmol. Astropart. Phys. 06 (2014) 030.

[37] K. P. Modak and D. Majumdar, Confronting Galactic and extragalactic γ rays observed by Fermi-lat with annihilating dark matter in an inert Higgs doublet model, Astrophys. J. Suppl. Ser. **219**, 37 (2015).

[38] M. Gustafsson, The inert doublet model and its phenomenology, *Proc. Sci.*, CHARGED2010 (2010) 030.

[39] M. Hashemi, M. Krawczyk, S. Najjari, and A. F. Żarnecki, Production of inert scalars at the high energy e^+e^- colliders, J. High Energy Phys. 02 (2016) 187.

[40] M. Aoki, S. Kanemura, and H. Yokoya, Reconstruction of inert doublet scalars at the International Linear Collider, Phys. Lett. B **725**, 302 (2013).
[41] P. M. Ferreira and B. Swiezewska, One-loop contributions to neutral minima in the inert doublet model, J. High Energy Phys. 04 (2016) 099.
[42] P. M. Ferreira and B. Swiezweska, One-loop inert and pseudo-inert minima, arXiv:1506.00585.
[43] A. Ilnicka, M. Krawczyk, and T. Robens, Constraining the inert doublet model, arXiv:1505.04734.
[44] B. Swiezewska, Inert scalars and vacuum metastability around the electroweak scale, J. High Energy Phys. 07 (2015) 118.
[45] M. Krawczyk, D. Sokoowska, P. Swaczyna, and B. Swieewska, Higgs $\to \gamma\gamma$, $Z\gamma$ in the inert doublet model, Acta Phys. Pol. B **44**, 2163 (2013).
[46] B. Gorczyca and M. Krawczyk, New results for the inert doublet model, Acta Phys. Pol. B **42**, 2229 (2011); Erratum, Acta Phys. Pol. B **43**, 481(E) (2012).
[47] N. Khan and S. Rakshit, Constraints on inert dark matter from the metastability of the electroweak vacuum, Phys. Rev. D **92**, 055006 (2015).
[48] A. Ilnicka, M. Krawczyk, and T. Robens, Inert doublet model in light of LHC run 1 and astrophysical data, Phys. Rev. D **93**, 055026 (2016).
[49] N. Chakrabarty, D. K. Ghosh, B. Mukhopadhyaya, and I. Saha, Dark matter, neutrino masses, and high scale validity of an inert Higgs doublet model, Phys. Rev. D **92**, 015002 (2015).
[50] A. Belyaev, G. Cacciapaglia, I. P. Ivanov, F. Rojas, and M. Thomas, Anatomy of the inert two Higgs doublet model in the light of the LHC and non-LHC dark matter searches, arXiv:1612.00511.
[51] B. W. Lee, C. Quigg, and H. B. Thacker, Weak interactions at very high-energies: The role of the Higgs boson mass, Phys. Rev. D **16**, 1519 (1977).
[52] A. Arhrib, R. Benbrik, and N. Gaur, $H \to \gamma\gamma$ in inert Higgs doublet model, Phys. Rev. D **85**, 095021 (2012).
[53] B. Grinstein, C. W. Murphy, and P. Uttayarat, One-loop corrections to the perturbative unitarity bounds in the *CP*-conserving two-Higgs doublet model with a softly broken $\mathbb{Z}_2$ symmetry, J. High Energy Phys. 06 (2016) 070.
[54] V. Cacchio, D. Chowdhury, O. Eberhardt, and C. W. Murphy, Next-to-leading order unitarity fits in two-Higgs-doublet models with soft $\mathbb{Z}_2$ breaking, J. High Energy Phys. 11 (2016) 026.
[55] M. E. Peskin and T. Takeuchi, Estimation of oblique electroweak corrections, Phys. Rev. D **46**, 381 (1992).
[56] R. Barbieri, L. J. Hall, and V. S. Rychkov, Improved naturalness with a heavy Higgs: An alternative road to LHC physics, Phys. Rev. D **74**, 015007 (2006).
[57] M. Baak, J. Cúth, J. Haller, A. Hoecker, R. Kogler, K. Mönig, M. Schott, and J. Stelzer (Gfitter Group), The global electroweak fit at NNLO and prospects for the LHC and ILC, Eur. Phys. J. C **74**, 3046 (2014).
[58] A. Djouadi, The Anatomy of electro-weak symmetry breaking: II. The Higgs bosons in the minimal supersymmetric model, Phys. Rep. **459**, 1 (2008).
[59] B. Swiezewska and M. Krawczyk, Diphoton rate in the inert doublet model with a 125 GeV Higgs boson, Phys. Rev. D **88**, 035019 (2013).
[60] M. Krawczyk, D. Sokolowska, P. Swaczyna, and B. Swiezewska, Constraining inert dark matter by $R_{\gamma\gamma}$ and WMAP data, J. High Energy Phys. 09 (2013) 055.
[61] G. Aad *et al.* (ATLAS Collaboration), Measurement of Higgs boson production in the diphoton decay channel in pp collisions at center-of-mass energies of 7 and 8 TeV with the ATLAS detector, Phys. Rev. D **90**, 112015 (2014).
[62] V. Khachatryan *et al.* (CMS Collaboration), Observation of the diphoton decay of the Higgs boson and measurement of its properties, Eur. Phys. J. C **74**, 3076 (2014).
[63] A. Goudelis, B. Herrmann, and O. Stål, Dark matter in the inert doublet model after the discovery of a Higgs-like boson at the LHC, J. High Energy Phys. 09 (2013) 106.
[64] A. Pierce and J. Thaler, Natural dark matter from an unnatural Higgs boson and new colored particles at the TeV scale, J. High Energy Phys. 08 (2007) 026.
[65] E. Lundström, M. Gustafsson, and J. Edsjö, The inert doublet model and LEP II limits, Phys. Rev. D **79**, 035013 (2009).
[66] Q. H. Cao, E. Ma, and G. Rajasekaran, Observing the dark scalar doublet and its impact on the Standard-Model Higgs boson at colliders, Phys. Rev. D **76**, 095011 (2007).
[67] K. Griest and D. Seckel, Three exceptions in the calculation of relic abundances, Phys. Rev. D **43**, 3191 (1991).
[68] F. S. Queiroz and C. E. Yaguna, The CTA aims at the inert doublet model, J. Cosmol. Astropart. Phys. 02 (2016) 038.
[69] A. Alloul, N. D. Christensen, C. Degrande, C. Duhr, and B. Fuks, `FeynRules 2.0`: A complete toolbox for tree-level phenomenology, Comput. Phys. Commun. **185**, 2250 (2014).
[70] G. Belanger, F. Boudjema, P. Brun, A. Pukhov, S. Rosier-Lees, P. Salati, and A. Semenov, Indirect search for dark matter with `micrOMEGAs 2.4`, Comput. Phys. Commun. **182**, 842 (2011); G. Belanger, F. Boudjema, A. Pukhov, and A. Semenov, `micrOMEGAs_3`: A program for calculating dark matter observables, Comput. Phys. Commun. **185**, 960 (2014).
[71] A. Belyaev, N. D. Christensen, and A. Pukhov, `CalcHEP 3.4` for collider physics within and beyond the Standard Model, Comput. Phys. Commun. **184**, 1729 (2013).
[72] T. Sjostrand, S. Mrenna, and P. Z. Skands, `PYTHIA 6.4` physics and manual, J. High Energy Phys. 05 (2006) 026.
[73] M. L. Mangano, M. Moretti, F. Piccinini, R. Pittau, and A. D. Polosa, `ALPGEN`, a generator for hard multiparton processes in hadronic collisions, J. High Energy Phys. 07 (2003) 001.
[74] M. L. Mangano, M. Moretti, F. Piccinini, and M. Treccani, Matching matrix elements and shower evolution for top-quark production in hadronic collisions, J. High Energy Phys. 01 (2007) 013; S. Hoeche, F. Krauss, N. Lavesson, L. Lonnblad, and M. Mangano, Matching parton showers and matrix elements, arXiv:hep-ph/0602031.
[75] M. Cacciari, G. P. Salam, and G. Soyez, FastJet user manual, Eur. Phys. J. C **72**, 1896 (2012).
[76] M. Cacciari, G. P. Salam, and G. Soyez, The anti-$k(t)$ jet clustering algorithm, J. High Energy Phys. 04 (2008) 063.

[77] G. Aad *et al.* (ATLAS Collaboration), Search for direct production of charginos and neutralinos in events with three leptons and missing transverse momentum in $\sqrt{s} = 8$ TeV pp collisions with the ATLAS detector, J. High Energy Phys. 04 (2014) 169.

[78] V. Khachatryan *et al.* (CMS Collaboration), Searches for electroweak neutralino and chargino production in channels with Higgs, Z, and W bosons in pp collisions at 8 TeV, Phys. Rev. D **90**, 092007 (2014).

[79] J. Pumplin, D. R. Stump, J. Huston, H. L. Lai, P. M. Nadolsky, and W. K. Tung, New generation of parton distributions with uncertainties from global QCD analysis, J. High Energy Phys. 07 (2002) 012.